CHEMISTRY OF MATERIALS

ARTICLE

pubs.acs.org/cm

High Density Germanium Nanowire Growth Directly from Copper Foil by Self-Induced Solid Seeding

Hugh Geaney,[†] Calum Dickinson,[†] Christopher A. Barrett,[†] and Kevin M. Ryan[†,‡,*]

[†]Materials and Surface Science Institute and Department of Chemical and Environmental Sciences, University of Limerick, Limerick, Ireland

[‡]SFI-Strategic Research Cluster in Solar Energy Research, University of Limerick, Limerick, Ireland

Supporting Information

ABSTRACT: Herein, we describe the growth of highly dense germanium nanowire mats directly on copper foil by a self-induced, solid seeded protocol. The existence of Cu_3Ge tips on each of the nanowires indicates that growth proceeds via a solid catalyzed route, dependent on the *in situ* formation of the germanide intermediate. The nanowires show a tight diameter distribution and typically ⟨110⟩ growth directions resulting from similarities in the *d* spacings between the nanowire and the catalyst seed. The nanowires and substrates were characterized using transmission electron microscopy (TEM), scanning electron microscopy (SEM), X-ray diffraction (XRD), scanning transmission electron microscopy (STEM), energy-dispersive X-ray spectroscopy (EDX), and electron backscatter diffraction (EBSD).

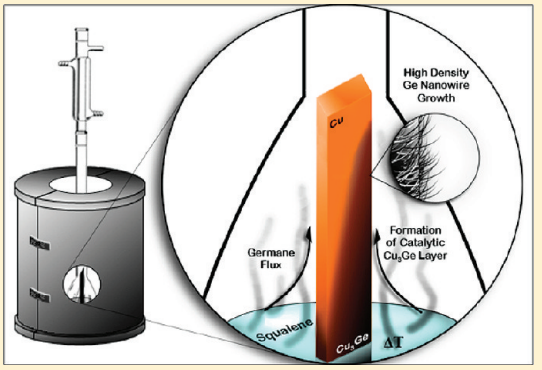

KEYWORDS: germanium, nanowire, solid phase seeding

INTRODUCTION

Germanium nanowires (Ge NWs) have found significant emerging applications spanning the solar, semiconductor, and storage industries.[1−5] The combination of high mobility and a large Bohr excitonic radius makes Ge NWs the semiconductor material of choice either for next generation, on-chip gate architectures or as p−n junction absorber arrays in photovoltaics.[1,2] Ge NWs have shown promise in Li battery anodes as a result of their ability to withstand volume expansion on lithium insertion coupled with high theoretical capacities (1600 mA h/g) and increased room temperature diffusivity (compared to Si).[3] The conventional seeding protocol where a metal nanoparticle forms a eutectic melt with the semiconductor has several advantages in forming NWs, particularly for discrete applications, as precise control over diameter and, in some cases, length is possible.[4−6] The metal seed acts as a sink for the growth species either as a liquid[7] (vapor liquid solid (VLS)) or as a solid[8−10] (vapor solid solid (VSS)) with work showing that the preferred orientations and defects in the metal seed can be transferred to the semiconductor NW.[11] Metal seeded growth has shifted toward solid catalysts consisting of Cu,[12] Ni,[13,14] and Fe[15] in an effort to limit the diffusion of metal atoms into the NWs associated with the use of Au, which can severely impact the electrical properties of the NWs.[16,17] The emergence of storage and photovoltaic applications places new demands on synthetic protocols for Ge NWs, with production directly from the current collector, in high yield and low cost, desirable. In directly seeded growth, high density is difficult to achieve, as temperature driven agglomeration can limit the number of catalytic sites available while also leading to a diameter spread in the NWs formed.[18−20]

The emergence of self-catalytic[15,21−25] growth systems for Ge NW formation has allowed high yield growth, often from low cost precursors.[26] Using the correct conditions, spontaneous NW formation with defect free morphologies and tight diameter distributions have been achieved.[27] Self-catalytic approaches (without the direct incorporation of discrete nanoparticle seeds) have also been successfully extended to the formation of Ge NWs directly on Fe,[15] Ta, and W substrates.[25] The most interesting candidate for NW growth is copper, because of its use as a current collector in lithium ion batteries. While VSS seeding from copper nanocrystals is known, direct growth from bulk copper would be very attractive, as it potentially offers a route toward binder free cells at low cost, with sufficient gravimetric density for commercial viability.[28−30]

Here, we present the highly dense growth of Ge NWs in a self-catalyzed process through the thermal decomposition of diphenylgermane (DPG) on copper foil in the vapor phase of a high boiling point solvent. The NWs are grown without the incorporation of discrete metal nanoparticles. Rather, we show that the *in situ* formation of Cu_3Ge acts as a catalyst for the formation of extremely dense NW mats with a very low diameter variation. This is the first direct observation of metal germanide tips in a self-induced, VSS process from bulk metals, offering important

Received: August 3, 2011
Revised: September 21, 2011
Published: October 06, 2011

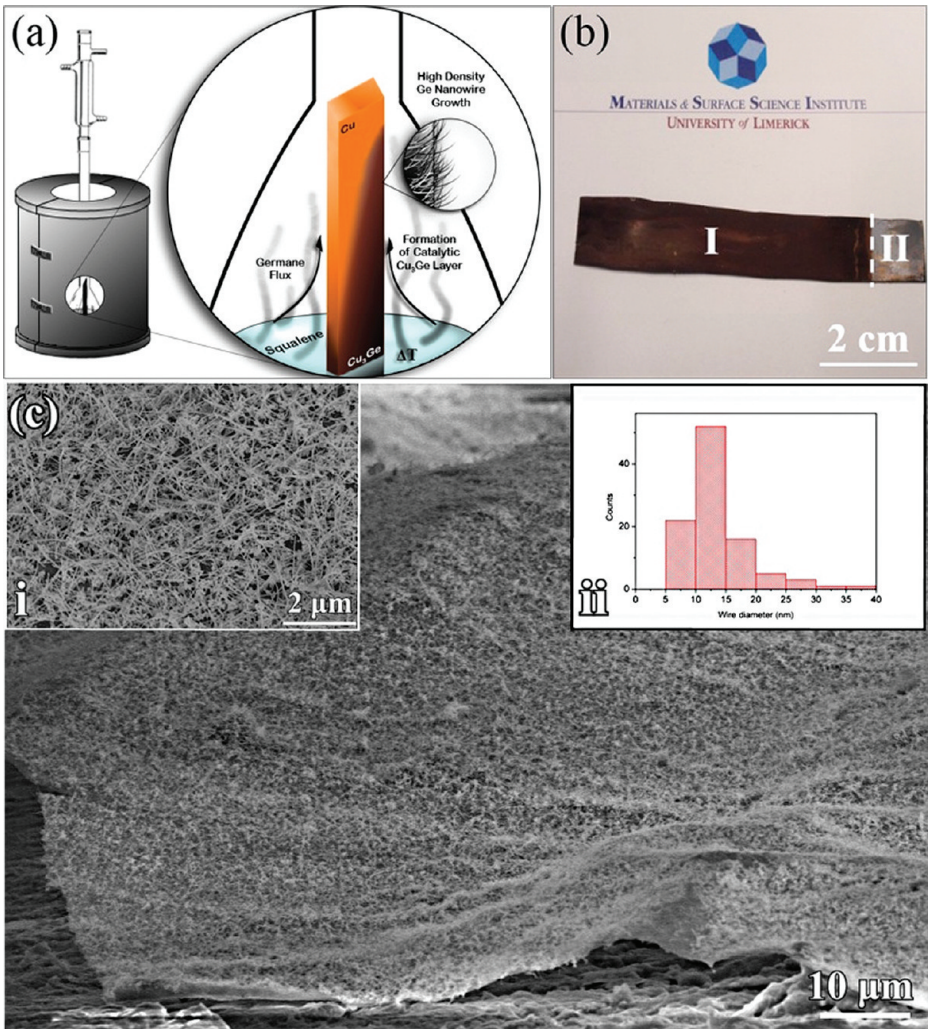

Figure 1. (a) Schematic outlining the NW growth system used. (b) Typical postsynthetic substrate showing the colors that correspond to the large scale NW coverage on area I and the Cu_3Ge layer in area II. (c) SEM image of the highly dense Ge NW mats grown on the Cu substrates. The underlying substrate can be seen in the foreground with inset I showing a higher magnification image of the Ge NW mats. The size distribution of the NWs can be seen in inset ii.

insights into this growth protocol. High resolution transmission electron microscopy (HRTEM) showed both ⟨110⟩ and ⟨112⟩ growth directions in the NW, with the preferential ⟨110⟩ growth directed by the orientation of the *in situ* generated orthorhombic Cu_3Ge nanocrystals.

II. EXPERIMENTAL SECTION

Substrate Preparation and Postsynthetic Treatment. Cu foil with a 0.25 mm thickness and 99.9% purity was purchased from Goodfellows. The Cu was cleaned with 0.1 M nitric acid and rinsed repeatedly with deionized water, and then, it was dried before introduction into the reactor setup. After reaction, the NW covered substrates were removed from the reaction flask. The substrates were rinsed with toluene to remove residual high boiling point solvent (HBS) and dried under a N_2 line prior to characterization.

Reaction Setup. Reactions were carried out using a modified procedure to that previously reported.[31] Squalene (5 mL; ≥98% Aldrich) was weighed into a custom-made Pyrex round bottomed flask. The Cu substrate was then placed into the flask, which was attached to a Schlenk line setup via a water condenser. This was then ramped to a temperature of 125 °C using a three zone furnace. A vacuum of at least 100 mTorr was applied for 1 h to remove moisture from the system. Following this, the system was purged with Ar. The flask was then ramped to the reaction temperature of 425 °C. Once the temperature had stabilized, 0.25 mL of DPG (>95% Gelest) was injected through a septum cap into the system. DPG is known to thermally decompose to germane at temperatures above 380 °C. Thus, germane dissolved in the squalene vapor is the NW monomer source.[32,33] A reaction time of 5 min was allowed to nucleate and grow the NWs. Then, the furnace was opened, and the setup was allowed to cool to room temperature before extracting the NW coated substrate.

Analysis. Scanning electron microscopy (SEM) analysis was performed on a Hitachi SU-70 system operating between 3 and 20 kV. The Cu foil substrates were untreated prior to SEM analysis. Electron backscatter diffraction (EBSD) was carried out at 20 kV and with a beam current of 1.54 nA, using an Oxford Instruments Nordlys EBSD detector and HKL Channel 5 software. For TEM analysis, the NWs were removed from the Cu substrates through the use of a sonic bath. TEM analysis was conducted using a 200 kV JEOL JEM-2100F field emission microscope equipped with a Gatan Ultrascan CCD camera and an EDAX Genesis EDS detector. Energy-dispersive X-ray spectroscopy (EDX) analysis of the NWs was conducted on Au TEM grids. X-ray

dx.doi.org/10.1021/cm202276m |*Chem. Mater.* 2011, 23, 4838–4843

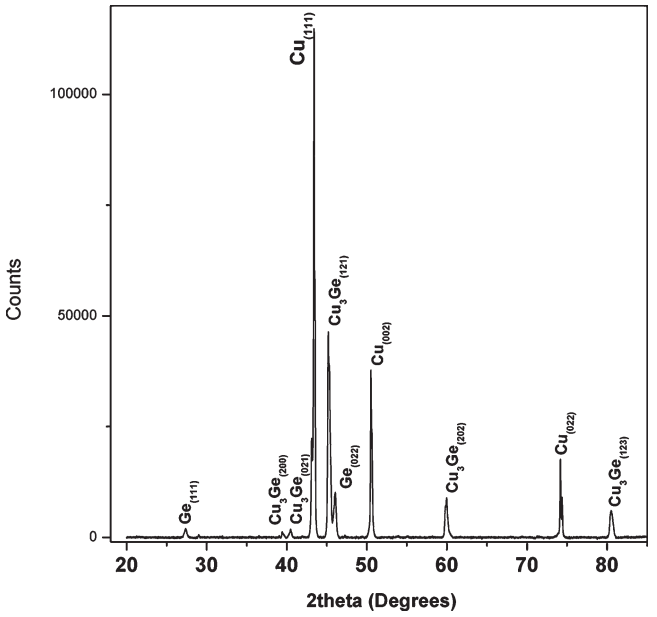

Figure 2. XRD pattern obtained from postsynthetic Ge NW covered substrate. The main Ge, Cu_3Ge, and Cu reflections present have been indexed.

diffraction (XRD) analysis was conducted using a PANalytical X'Pert PRO MRD instrument with a Cu Kα radiation source (λ = 1.5418 Å) and an X'celerator detector.

RESULTS AND DISCUSSION

Figure 1a shows a schematic of the setup for NW growth. The bulk copper substrate was placed vertically in an elongated round bottomed flask as shown, with squalene as the solvent. Seventy five percent of the substrate is above the liquid meniscus and therefore in the vapor phase of the high boiling point solvent during high temperature reflux.

Figure 1b shows a typical postsynthetic substrate from a reaction carried out at 425 °C. Following the reaction, the copper substrate within the vapor phase of the reactor (region I) was found to be a dark brown/purple color. In contrast, the portion of the substrate below the liquid meniscus (region II) was silver colored with a very distinct cut off line. HRSEM (Figure 1c) confirmed that the distinct coloration in region I was due to high density NW growth, which is completely selective to the vapor phase. The NWs can be seen to form in extremely dense meshes which extend over large areas. Here, the NWs were viewed from near the edge of the copper, allowing the underlying substrate to be identified in the foreground of the image. The inset (i), a higher magnification image, shows that the NWs are untapered along their length and extend to several micrometers in length. Additional images showing the mat-like nature and high density of the NWs grown directly on the copper are provided in Figure S1 in the Supporting Information. The diameter distribution shown in Figure 1c inset (ii) was taken from a count of 100 NWs across different reactions using TEM and shows an average diameter of 13.4 nm and a standard deviation of 5.2 nm. Interestingly, outliers with diameters >25 nm were found to exhibit tortuosity (Figure S2 in the Supporting Information) due to a diameter-dependent increase in NW kinking caused by defect driven growth direction changes.[27]

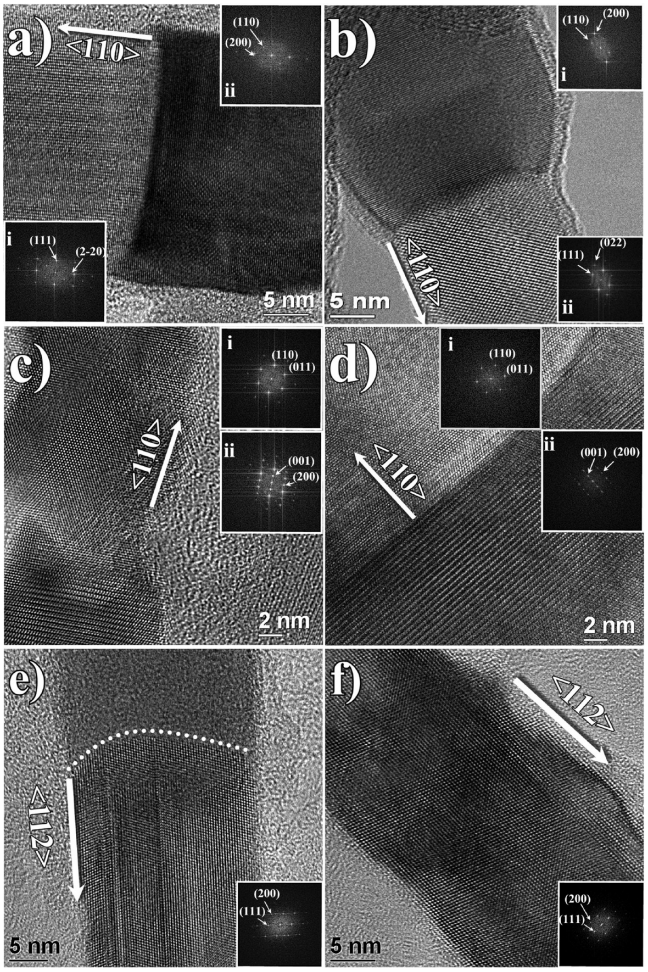

Figure 3. HRTEM analysis of Ge NWs showing ⟨110⟩ growth directions. (a) High resolution interface of a Ge NW. The FFT insets (i) and (ii) are indexed with spots that correspond to the diamond cubic Ge and the orthorhombic Cu_3Ge seed. (b) Interfacial region of a ⟨110⟩ NW and a Cu_3Ge seed. The indexed FFT insets (i) and (ii) correspond to the diamond cubic Ge NW and orthorhombic Cu_3Ge seed, respectively. (c) Additional example of a ⟨110⟩ NW with a lattice resolved NW/seed interface. The FFT insets (i) and (ii) again belong to the NW and seed, respectively. (d) High resolution interface of a NW and Cu_3Ge seed. (e and f) HRTEM images of Ge NWs with the less common ⟨112⟩ growth directions. The NW in part e shows longitudinal faults commonly associated with NWs showing ⟨112⟩ growth directions. The interface between the NW and the catalyst seed particle is shown by the dotted line. (f) Perfect single crystal NW with a ⟨112⟩ growth direction.

The XRD diffractogram, shown in Figure 2, taken from a typical Ge NW covered Cu substrate, is indexed with the expected peaks of Cu and Ge. Interestingly, additional peaks that are consistent with Cu_3Ge were also observed. The Cu peaks, attributed to cubic Cu with space group $Fm\bar{3}m$ and cell parameter 3.6150 Å, remain unchanged when compared to the starting Cu substrate (Figure S3a in the Supporting Information). The Ge NWs were found to exist in the diamond cubic form with the $Fd\bar{3}m$ space group and cell parameter 5.623 Å. The Cu_3Ge was present in orthorhombic form with space group *Pmmn* and cell parameters a = 4.578 Å, b = 5.272 Å, and c = 4.204 Å. The presence of Cu_3Ge on the growth substrates is noteworthy because it suggests that the formation of this alloy is a

dx.doi.org/10.1021/cm202276m |*Chem. Mater.* 2011, 23, 4838–4843

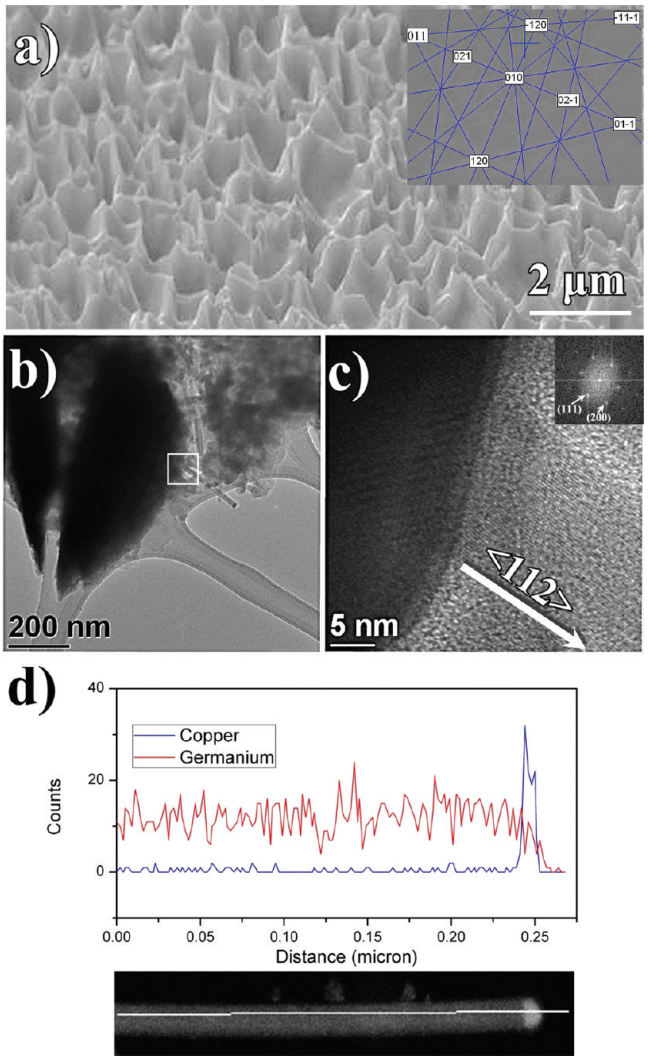

Figure 4. (a) Growth substrate after NW removal with inset EBSD pattern confirming that the layer is composed exclusively of Cu_3Ge. (b) Dark Cu_3Ge island with attached Ge NWs. (c) HRTEM image taken from the highlighted NW in part b showing the orientation of the ⟨112⟩ NW to the Cu_3Ge island. (d) EDX line profile analysis of a single NW showing Ge and Cu signals. The inset STEM image shows the NW analyzed.

facilitating step in NW formation. Cu_3Ge formation was characterized by XRD in all reactions carried out following this protocol. It was found that the Ge NWs could be removed from the growth substrates by sonication while still retaining the integrity of the Cu_3Ge layer (Figure S3b in the Supporting Information).

A TEM survey found that each NW possessed a catalyst particle on one end with approximately 95% of the NWs growing along the ⟨110⟩ axis and the remaining 5% showing ⟨112⟩ growth directions. The presence of Cu_3Ge tips on the NWs confirms they are formed via a solid seeding mechanism, as NW growth was conducted far below the Cu/Ge eutectic point of 644 °C.[34] The irregular seed geometry observed here has previously been noted for Cu_3Ge seeded Ge NWs[12] and is in contrast to the typically observed, hemispherical seeds for Au seeded NWs.[32] Upon closer inspection, it was found that the Cu_3Ge catalyst seeds had two specific orientations relative to the ⟨110⟩ NWs. The interfacial region between a ⟨110⟩ NW and the Cu_3Ge catalyst seed can be seen in Figure 3a. Inset (i) is an indexed fast Fortier transform (FFT) showing spots consistent with the (111) and $(2\bar{2}0)$ spacings of diamond cubic Ge. The image was taken down the $[11\bar{2}]$ zone axis and indicates a ⟨110⟩ growth direction for the NW. The FFT in inset (ii) is indexed for orthorhombic Cu_3Ge. In Figure 3 b, the NW shows a ⟨110⟩ growth direction and was viewed down the $[0\bar{1}1]$ zone axis. In both part a and part b of Figure 3, the heteroepitaxial relationship between the seed and the NW was found to be $[100]_{seed}/[110]_{NW}$. This relationship is likely facilitated by the similarity of the respective *d* spacings (0.2289 and 0.2000 nm for (200) and (220) of the seed and NW, respectively). The other seed/NW relationship noted (Figure 3c and d) was found to be $[001]_{seed}/[110]_{NW}$, which is again facilitated by the (002) lattice spacing of Cu_3Ge (0.2102 nm) being approximately equal to the (022) spacing of germanium (0.2000 nm). The indexed FFT in Figure 3c inset (i) is viewed down the [111] zone axis. The FFT in inset (ii) shows that the NW here is orientated to the (001) plane of the Cu_3Ge seed. A higher magnification of the interface between a NW and seed with the same orientation is presented in Figure 3d. An image of an individual orthorhombic Cu_3Ge catalyst tip found at the end of a ⟨110⟩ NW and additional TEM images of NWs showing ⟨110⟩ growth directions can be found in Figure S4 in the Supporting Information. NWs with ⟨112⟩ growth directions were found to make up the remaining 5% of the typical product. The scarcity of this growth direction is consistent with previous seeded approaches, giving similar growth direction distributions.[35,36] Two high resolution images of ⟨112⟩ NWs can be seen in parts e and f of Figure 3. Interestingly, the NW in Figure 3e shows longitudinal faults that continue to the seed. These faults result in a streaking in the inset FFT.[27] Figure 3f is a defect free NW with a ⟨112⟩ growth direction. As a result of the scarcity of ⟨112⟩ NWs, we were unable to obtain a high resolution image of the NW seed; however, it is likely that the seed orientation is $[200]_{seed}/[112]_{NW}$ due to the similarity in the *d* spacings of (400) and (224) (0.1145 nm and 0.1155 nm, respectively).

The SEM analysis of the starting Cu foil and bare postsynthetic substrates (Figure S5 in the Supporting Information) showed that the formation of catalytic Cu_3Ge leads to substantial roughening of the substrate. The image presented in Figure 4a was taken at a 70° tilt angle, with tilt compensation, to allow simultaneous EBSD analysis. The EBSD point analysis (inset) confirmed that the composition of the entire surface was undulating islands of orthorhombic Cu_3Ge. The unindexed EBSD pattern is shown in Figure S6 in the Supporting Information. Investigation of the topology and composition of region II of a postsynthetic substrate, as presented in Figure 1b, using SEM and EBSD analysis (Figure S7 in the Supporting Information), showed the formation of more isolated, crystalline Cu_3Ge islands on top of the underlying Cu substrate.[37] Having confirmed the large scale presence of Cu_3Ge as a postsynthetic layer on the growth substrates, a sample with dense NW coverage was doctor bladed and placed on a TEM grid to investigate the relationship between the NWs and the catalytic layer. Figure 4b shows a large region of excised Cu_3Ge with Ge NWs attached. The HRTEM image of the NW in Figure 4c shows the NW growing directly from the Cu_3Ge. The inset FFT shows that the NW possesses a ⟨112⟩ growth direction. HRTEM images of a portion of the Cu_3Ge layer showed the presence of polycrystalline domains (Figure S8 in the Supporting Information). Line profile EDX

dx.doi.org/10.1021/cm202276m |*Chem. Mater.* 2011, 23, 4838–4843

analysis conducted on the single NW shown in the scanning transmission electron microscopy (STEM) image (inset) is presented in Figure 4d. The confinement of Cu to the catalyst tip and the nonzero Ge signal present (with Cu to Ge ratio of approximately 3:1) again confirm that the tip is composed of Cu_3Ge.

The presence of Cu_3Ge tips on the NWs is a clear indicator that a VSS mechanism is responsible for the subeutectic growth presented (Cu/Ge eutectic point exists at 644 °C[34]). We have shown that two specific seed orientations are responsible for the ⟨110⟩ grown NWs, which is important given the recent interest in the transfer of crystallographic information from solid catalyst seeds to the resultant NWs.[11] While subeutectic, orthorhombic Cu_3Ge catalyzed, Ge NWs have been synthesized from sputtered Cu layers,[12,38] our report details the first subeutectic growth from bulk Cu. The dominance of ⟨110⟩ growth is consistent with these previous reports detailing Cu_3Ge seeded Ge NWs. However, the self-induced, solid seeding noted here is unique when compared to other Cu seeded approaches, as the catalyst seed is an intermediate formed during precursor decomposition on the metal growth substrate. The term "self-induced" refers to the fact that no discrete metal nanoparticles are introduced into the reaction setup at any stage and the Cu_3Ge catalyst particles are formed *in situ*. While NW growth from other metal substrates without the incorporation of discrete metal particles has previously been reported,[15,39] there appears to be noticeable mechanistic differences from those presented here. Previously, Ge NW growth from bulk Fe substrates via a root seeded mechanism was proposed to be due to the formation of a transition metal rich alloy (Fe_3Ge); however, no metal catalyst particles were found on the NWs after removal from the substrate.[15] Here, the presence of catalytic tips, which were unambiguously identified as Cu_3Ge, on the NWs after removal from the substrate shows that seed sizes of 5 to 40 nm are necessarily formed during decomposition of the DPG in the vapor phase of the organic medium. Although the formation of these seeds cannot be identified *in situ*, the lattice mismatch between the Cu and Cu_3Ge is sufficient that the growing Cu_3Ge would proceed initially through the formation of isolated catalytic islands that subsequently grow into the polycrystalline Cu_3Ge layer noted postsythesis here and elsewhere.[40] While there is also a lattice mismatch between the Cu_3Ge seeds and the Ge NWs, an atomically sharp interface is produced as a result of the increased tolerance of lattice mismatch in 1D growth systems.[41,42] This accommodation of lattice mismatch in 1D systems likely encourages VSS driven, 1D NW growth parallel to additional Cu_3Ge formation on the substrate. The NW diameter is thus determined by the point in Cu_3Ge formation where, upon further monomer supply, 1D Ge growth becomes favored over additional Cu_3Ge formation on the substrate. This allows the high density formation of NWs within the critical diameter range noted.

The high density growth of Ge NW mats directly on a conductive Cu_3Ge layer atop a Cu substrate ensures that they are a promising candidate for applications where high density, bound NWs are required, such as Li battery anodes.[28] The intermetallic Cu_3Ge, which has excellent electrical properties, has recently been used as an efficient interconnect in Ge NW transistors, ensuring good electrical contact between the Cu and the Ge NWs here.[41,43] While the *in situ* formation of diffusion formed orthorhombic Cu_3Ge at 300 °C has been reported,[41,44] ours represents the first report of Cu_3Ge formed from the reaction of solid Cu foil and a vapor phase Ge reactant. A similar formation of a catalytic metal germanide layer followed by spontaneous NW nucleation may be possible in other germanide forming metals such as Co and Ni.

CONCLUSIONS

We have presented the growth of highly dense, crystalline Ge NWs on Cu substrates through a self-induced, solid seeding process, without the use of discrete metal nanocrystal catalysts. The NW growth proceeded on Cu through the spontaneous formation of a catalytic Cu_3Ge seeds within a Cu_3Ge layer upon exposure to Ge monomer. The layer was thoroughly characterized using EBSD and XRD analyses and was found to be orthorhombic Cu_3Ge identical to that noted on the NW tips, as characterized by TEM and EDX. The NWs formed were found to exhibit predominantly ⟨110⟩ growth directions and possessed a low diameter spread given the absence of predefined catalyst particles. The seeding process was facilited by similarities in *d* spacings between the orthorhombic Cu_3Ge and the cubic Ge NWs. This report gives an insight into the potential for high quality Ge NW growth from germanide forming metals.

ASSOCIATED CONTENT

Supporting Information. SEM and EBSD analysis of Ge reaction carried out at 375 °C showing Cu_3Ge island formation. Additional SEM images of dense Ge NWs grown directly on Cu. High resolution TEM image of kinked Ge nanowire. Unindexed EBSD pattern of a Cu_3Ge substrate. XRD patterns and SEM images taken from the initial Cu substrates and postsynthetic substrates with Ge NWs removed. Additional TEM images of NWs with ⟨110⟩ growth directions. TEM images of the excised Cu_3Ge. This material is available free of charge via the Internet at http://pubs.acs.org.

AUTHOR INFORMATION

Corresponding Author
*E-mail: Kevin.M.Ryan@ul.ie.

ACKNOWLEDGMENT

This work was supported principally by Science Foundation Ireland (SFI) under the Principal Investigator Program under Contract No. 06/IN.1/I85 and also by the Advanced Biomimetic Materials for Solar Energy Conversion Strategic Research Cluster (Contract No. 07/SRC/B1160). This work was also conducted under the framework of the INSPIRE program, funded by the Irish Government's Programme for Research in Third Level Institutions, Cycle 4, National Development Plan 2007−2013. Funding is acknowledged under the Irish Research Council for Science, Engineering, and Technology (IRCSET) embark initiative for H.G. H.G. would like to acknowledge Dr. Robert D. Gunning, Dr. Edric Gill, and Joe Murphy for useful scientific discussions.

REFERENCES

(1) Adhikari, H.; Marshall, A. F.; Chidsey, C. E. D.; McIntyre, P. C. *Nano Lett.* **2006**, *6*, 318–323.
(2) Liang, G.; Xiang, J.; Kharche, N.; Klimeck, G.; Lieber, C. M.; Lundstrom, M. *Nano Lett.* **2007**, *7*, 642–646.
(3) Chan, C. K.; Zhang, X. F.; Cui, Y. *Nano Lett.* **2007**, *8*, 307–309.

(4) Holmes, J. D.; Johnston, K. P.; Doty, R. C.; Korgel, B. A. *Science* **2000**, *287*, 1471–1473.
(5) Lu, X.; Hanrath, T.; Johnston, K. P.; Korgel, B. A. *Nano Lett.* **2002**, *3*, 93–99.
(6) Park, W. I.; Zheng, G.; Jiang, X.; Tian, B.; Lieber, C. M. *Nano Lett.* **2008**, *8*, 3004–3009.
(7) Wagner, R. S.; Ellis, W. C. *Appl. Phys. Lett.* **1964**, *4*, 89.
(8) Kodambaka, S.; Tersoff, J.; Reuter, M. C.; Ross, F. M. *Science* **2007**, *316*, 729–732.
(9) Tuan, H.-Y.; Lee, D. C.; Korgel, B. A. *Angew. Chem.* **2006**, *118*, 5308–5311.
(10) Kamins, T. I.; Williams, R. S.; Basile, D. P.; Hesjedal, T.; Harris, J. S. *J. Appl. Phys.* **2001**, *89*, 1008–1016.
(11) Barth, S.; Boland, J. J.; Holmes, J. D. *Nano Lett.* **2011**, *11*, 1550–1555.
(12) Kang, K.; Kim, D. A.; Lee, H.-S.; Kim, C.-J.; Yang, J.-E.; Jo, M.-H. *Adv. Mater.* **2008**, *20*, 4684–4690.
(13) Tuan, H.-Y.; Lee, D. C.; Hanrath, T.; Korgel, B. A. *Chem. Mater.* **2005**, *17*, 5705–5711.
(14) Barth, S.; Kolesnik, M. M.; Donegan, K.; Krstic, V.; Holmes, J. D. *Chem. Mater.* **2011**, *23*, 3335–3340.
(15) Mathur, S.; Shen, H.; Sivakov, V.; Werner, U. *Chem. Mater.* **2004**, *16*, 2449–2456.
(16) Allen, J. E.; Hemesath, E. R.; Perea, D. E.; Lensch-Falk, J. L.; LiZ., Y; Yin, F.; Gass, M. H.; Wang, P.; Bleloch, A. L.; Palmer, R. E.; Lauhon, L. J. *Nat. Nano.* **2008**, *3*, 168–173.
(17) Bailly, A.; Renault, O.; Barrett, N.; Zagonel, L. F.; Gentile, P.; Pauc, N.; Dhalluin, F.; Baron, T.; Chabli, A.; Cezar, J. C.; Brookes, N. B. *Nano Lett.* **2008**, *8*, 3709–3714.
(18) Hanrath, T.; Korgel, B. A. *J. Am. Chem. Soc.* **2002**, *124*, 1424–1429.
(19) Stelzner, T.; Andra, G.; Wendler, E.; Wesch, W.; Scholz, R.; Gosele, U.; Christiansen, S. *Nanotechnology* **2006**, *17*, 2895–2898.
(20) Jagannathan, H.; Deal, M.; Nishi, Y.; Woodruff, J.; Chidsey, C.; McIntyre, P. C. *J. Appl. Phys.* **2006**, 100.
(21) Gerung, H.; Boyle, T. J.; Tribby, L. J.; Bunge, S. D.; Brinker, C. J.; Han, S. M. *J. Am. Chem. Soc.* **2006**, *128*, 5244–5250.
(22) Hobbs, R. G.; Barth, S.; Petkov, N.; Zirngast, M.; Marschner, C.; Morris, M. A.; Holmes, J. D. *J. Am. Chem. Soc.* **2010**, *132*, 13742–13749.
(23) Zaitseva, N.; Harper, J.; Gerion, D.; Saw, C. *Appl. Phys. Lett.* **2005**, *86*, 053105–053105—3.
(24) Kim, B.-S.; Koo, T.-W.; Lee, J.-H.; Kim, D. S.; Jung, Y. C.; Hwang, S. W.; Choi, B. L.; Lee, E. K.; Kim, J. M.; Whang, D. *Nano Lett.* **2009**, *9*, 864–869.
(25) Drinek, V.; Fajgar, R.; Klementova, M.; Subrt, J. *J. Electrochem. Soc.* **2010**, *157*, K218–K222.
(26) Ge, M.; Liu, J. F.; Wu, H.; Yao, C.; Zeng, Y.; Fu, Z. D.; Zhang, S. L.; Jiang, J. Z. *J. Phys. Chem. C* **2007**, *111*, 11157–11160.
(27) Geaney, H.; Dickinson, C.; Weng, W.; Kiely, C. J.; Barrett, C. A.; Gunning, R. D.; Ryan, K. M. *Cryst. Growth Des.* **2011**, *11*, 3266–3272.
(28) Lahiri, I.; Oh, S.-W.; Hwang, J. Y.; Cho, S.; Sun, Y.-K.; Banerjee, R.; Choi, W. *ACS Nano* **2010**, *4*, 3440–3446.
(29) Lai, C.-H.; Huang, K.-W.; Cheng, J.-H.; Lee, C.-Y.; Hwang, B.-J.; Chen, L.-J. *J. Mater. Chem.* **2010**, *20*, 6638–6645.
(30) Xue, X.-Y.; Yuan, S.; Xing, L.-L.; Chen, Z.-H.; He, B.; Chen, Y.-J. *Chem. Commun.* **2011**, *47*, 4718–4720.
(31) Barrett, C. A.; Geaney, H.; Gunning, R. D.; Laffir, F. R.; Ryan, K. M. *Chem. Commun.* **2011**, *47*, 3843–3845.
(32) Chockla, A. M.; Korgel, B. A. *J. Mater. Chem.* **2009**, *19*, 996–1001.
(33) Collins, G.; Kolesnik, M.; Krstic, V.; Holmes, J. D. *Chem. Mater.* **2011**, *23*, 5235–5243.
(34) Fuller, C. S.; Struthers, J. D.; Ditzenberger, J. A.; Wolfstirn, K. B. *Phys. Rev.* **1954**, *93*, 1182–1189.
(35) Hanrath, T.; Korgel, B. A. *Small* **2005**, *1*, 717–721.
(36) Tuan, H.-Y.; Korgel, B. A. *Chem. Mater.* **2008**, *20*, 1239–1241.
(37) The lack of NW growth in this solution phase of the organic medium is consistent with our previous results, where the boiling point of the medium (385 °C) was insufficient to facilitate NW growth.[31] Reactions conducted at temperatures below 400 °C led to the formation of a homogeneous Cu_3Ge layer over the entire substrate.
(38) Kang, K.; Gu, G. H.; Kim, D. A.; Park, C. G.; Jo, M.-H. *Chem. Mater.* **2008**, *20*, 6577–6579.
(39) Barrett, C. A.; Gunning, R. D.; Hantschel, T.; Arstila, K.; O'Sullivan, C.; Geaney, H.; Ryan, K. M. *J. Mater. Chem.* **2010**, *20*, 135–144.
(40) Chao, Y. L.; Xu, Y.; Scholz, R.; Woo, J. C. S. *IEEE Electron Device Lett.* **2006**, *27*, 549–551.
(41) Burchhart, T.; Lugstein, A.; Hyun, Y. J.; Hochleitner, G.; Bertagnolli, E. *Nano Lett.* **2009**, *9*, 3739–3742.
(42) Burchhart, T.; Zeiner, C.; Hyun, Y. J.; Lugstein, A.; Hochleitner, G.; Bertagnolli, E. *Nanotechnology* **2010**, *21*, 5.
(43) Darling, K. A.; Guduru, R. K.; Reynolds, C. L.; Bhosle, V. M.; Chan, R. N.; Scattergood, R. O.; Koch, C. C.; Naravan, J.; Aboelfotoh, M. O. *Intermetallics* **2008**, *16*, 378–383.
(44) Zeiner, C.; Lugstein, A.; Burchhart, T.; Pongratz, P.; Connell, J. G.; Lauhon, L. J.; Bertagnolli, E. *Nano Lett.* **2011**, *11*, 3108–3112.